03,04,07,08

Generation of clusterized structure of $La_{0.7}Sr_{0.3}MnO_{3-x}$ films in magnetron plasma: Effect of electric fields and ion sound on particle levitation and „frozen“ oscillations of film parameters

© V.D. Okunev, Z.A. Samoilenko, Yu.M. Nikolaenko, T.A. Dyachenko, V.V. Burkhovetski, A.S. Korneevets

Galkin Donetsk Institute for Physics and Engineering,
Donetsk, Russia

E-mail: vladimir.okunev2010@mail.ru

Received November 6, 2024
Revised November 6, 2024
Accepted December 6, 2024

The influence of clusters of different sizes ($D = 50-400$ Å) formed in magnetron plasma on the structure and properties of 36 samples of $La_{0.7}Sr_{0.3}MnO_{3-x}$ films deposited on glass along the particle flow was studied. As a result of comparing the „frozen“ oscillations of film parameters with real ion-acoustic oscillations in the plasma, the scenario of its clusterization, which is impossible without particle levitation, was reconstructed. A phenomenological description of this phenomenon is proposed. It is shown that at distances from the target $L \leq 2.15$ cm, flow clustering is limited by the levitation of atomic clusters as a result of the balance between gravity, ion sound pressure and the force of interaction of charged particles with electric fields; the contribution of ion sound to particle levitation here does not exceed 12%. In the absence of an electric field ($L \geq 2.45$ cm), levitation depends only on the entrainment of particles by ion-sound oscillations. The results of calculating the critical sizes of levitating atomic groups are consistent with experiment. The influence of changes in the charge state of manganese ions along the flow of particles on the formation of the cluster structure of films has been studied. In the range of $2.15 < L < 2.45$ cm, where the cluster size decreases by half, the relationship between the electrical properties of the films and their structure changes qualitatively. For clusters with sizes smaller than the Debye screening radius ($l_D = 175 \mp 30$ Å), the size effects observed in the samples are consistent with the model of localization of electronic states proposed by Lifshitz.

Keywords: magnetron plasma, manganese ions of different valences, flow clustering, particle levitation, ion-acoustic wave, amorphous $La_{0.7}Sr_{0.3}MnO_3$ films.

DOI: 10.61011/PSS.2025.01.60586.295

1. Introduction

Magnetron sputtering of targets is one of the main methods of low-temperature plasma generation and is widely used for the preparation of thin films [1,2] when it is possible to obtain fast results with low costs, especially in the case of complex multicomponent chemical compounds. Taking into account the experience of recent decades and numerous experimental works devoted to the production and study of films, we believe that the versatility of magnetron sputtering in relation to a wide variety of materials is associated with plasma clustering, which creates favorable conditions for film growth: atomic clusters formed in plasma with a large number of unsaturated bonds and high chemical activity ensure a minimum concentration of defects at the boundaries, facilitating the growth of films with a suitable experimental structure. The dust plasma is the link between these two directions (thin films and low-temperature plasma) [3,4]. This is a plasma containing dust particles up to several tens of microns in size. Particles are usually introduced from the outside, but they can also be formed during technological operations, thereby indirectly confirming the hypothesis outlined above. Such plasma is also of interest to specialists studying outer space.

At the same time, there is only a limited amount of experimental data on plasma clustering, which presumably has such a significant effect on the structure and properties of films, obtained mainly by sputtering metals [1–4]. The presence of heterovalent ions and the possibility of generating ion-sound vibrations complicate the problem for metal oxides, including $La_{0.7}Sr_{0.3}MnO_3$ [5–7].

It was generally understood based on the experimental data [6,7] that there are two stages of cluster formation in films: one begins in plasma and the other is realized already during the growth of the film on the substrate [7]. The presence of the first stage is confirmed by experimental data, mainly indirect:

- The cluster structures are always different under the same growth conditions for neighboring film sections with a width of 3 mm deposited along the particle flux, and the cluster sizes can significantly vary and have a different set of crystallographic structural groups [7].
- The intensities of coherent scattering characterizing the concentration of heterogeneous clusters for neighboring sites differ by 2–4 times [7].
- The observed deep modulation of the parameters of the cluster structure of films by ion-sound waves [7] is impossible during the growth of an already deposited film

on a substrate and can be realized only with plasma clusterization.

• Sufficiently large fragments of fractal structures are deposited on the substrates in the immediate vicinity of the target. These fragments are easily visible on images of the film surface in a scanning electron microscope [8].

The necessary energy for the implementation of the second stage is provided by electron and ion bombardment of the previously deposited layers with the loss of excess energy of the particles included in the film structure. The second stage is also stimulated by the action of the phase separation mechanisms [9–15] and is revealed experimentally. When large fragments are deposited on a substrate near the target, the kinetics of changes in the geometry of fractal structures can be directly observed in a scanning electron microscope [8]. However, it was not clear with the distance from the target where fractal structures no longer formed in what form the flow of sputtered material was deposited on the substrate and how the clustering process developed further. The lack of quantitative data — how the transition from one stage of film clustering to another stage is realized and when this transition begins — hinders the understanding and development of this interesting area. The main reason for this, in our opinion, is the lack of knowledge about the mechanisms of plasma clustering and the patterns of formation of a clustered film structure during the transition of a particle stream from a gaseous phase to a condensed one. As will be shown below, some of the effects observed in films were mistakenly attributed to the second stage of film growth, while in reality their occurrence is associated with the first stage.

The aim of the work was to obtain quantitative data on the formation of atomic groupings in a magnetron plasma, using primarily the results of studies of the structure and properties of deposited films. Taking into account possible factors determining the behavior of particles in a flux of sputtered material, the objective was to determine the nature of cluster formation in plasma, establish a relation between the first stage and the structure of layers deposited from the stream, and ultimately understand the mechanisms of film clustering. As a result, considering the features of the interaction of the particle flux with ion-sound waves and revealing the nature of „frozen“ oscillations in $La_{0.7}Sr_{0.3}MnO_{3-x}$ films, we found a relation between plasma clustering and particle levitation, attributable to their interaction with the internal fields of the magnetron and the entrainment by ion-sound waves, and thus solved the problem of the nature and mechanisms of the first stage of film clustering, eliminating the existing gap in understanding the nature of the universality of magnetron sputtering technology, thus confirming the hypothesis outlined above.

2. Research samples and experimental methods

$La_{0.7}Sr_{0.3}MnO_3$ target with a diameter of $D = 4$ cm was sputtered with a pulsed ($\tau \sim 3$ ms) voltage (350 V) on electrodes in a mixture of argon (84%) and oxygen (16%), with their full pressure $6 \cdot 10^{-3}$ and $1 \cdot 10^{-2}$ Torr [6]. The flow of the sprayed substance was deposited on a thin glass substrate 54 mm long, mounted along the flow of particles (Figure 1, *a*) interacting with the electric and magnetic fields of the magnetron (Figure 1, *b, c*). After deposition, this structure was divided into 18 separate 3 mm wide samples. A total of 36 samples were examined, prepared at two working gas pressures in the chamber for three ($6 \cdot 10^{-3}$ Torr) and six ($1 \cdot 10^{-2}$ Torr) hours. All figures show the average distances (L) of these samples from the target.

The structure of the samples, their electronic and optical properties were studied using standard equipment. X-ray microanalysis data and surface images of the samples in a scanning electron microscope were used to analyze the results. The characteristics of the magnetron plasma were studied using an electric probe, which makes it possible to measure local potential changes over a wide frequency range. Examples of such dependencies for four distances from the target are shown in Figure 1, *d*. On the oscillogram of the voltage pulse on the probe (Figure 1, *e*), the observed fluctuations have the character of noise oscillations (they are represented by a light strip at the top of the pulse (Figure 1, *e*), from which it is difficult to distinguish fluctuations of a certain frequency.

3. Results and discussion

The experimental results obtained in this work relate to the study of the structure, electrical and optical properties of $La_{0.7}Sr_{0.3}MnO_3$ films prepared by magnetron sputtering by comparing the data obtained with the Lifshitz model, with the results of the phenomenological description of particle levitation and measurements of the amplitude of vibrations potential in a low-temperature magnetron plasma (in the target sputtering operating mode), depending on the frequency and distance from the target.

3.1. Ion sound in magnetron plasma and „frozen“ oscillations in the cluster structure of deposited films

The activation of the discharge is accompanied by the appearance of a negative differential resistance (NDR) of *S*-type section on the current-voltage curve (CVC) of the magnetron and the generation of voltage oscillations on the electrodes. In the presence of ions in the flow, these vibrations excite longitudinal ion-sound waves [5–7].

As can be seen from Figure 1, *d*, fluctuations are observed in a wide frequency range and, basically, have the character of noise oscillations, showing that a guaranteed increase of fluctuations in the CVC section with NDR does not necessarily lead to regular fluctuations of a certain frequency (Figure 1, *e*). At the same time, measurements of the local potential in the plasma at various frequencies show the presence of sinusoidal potential changes with distance from

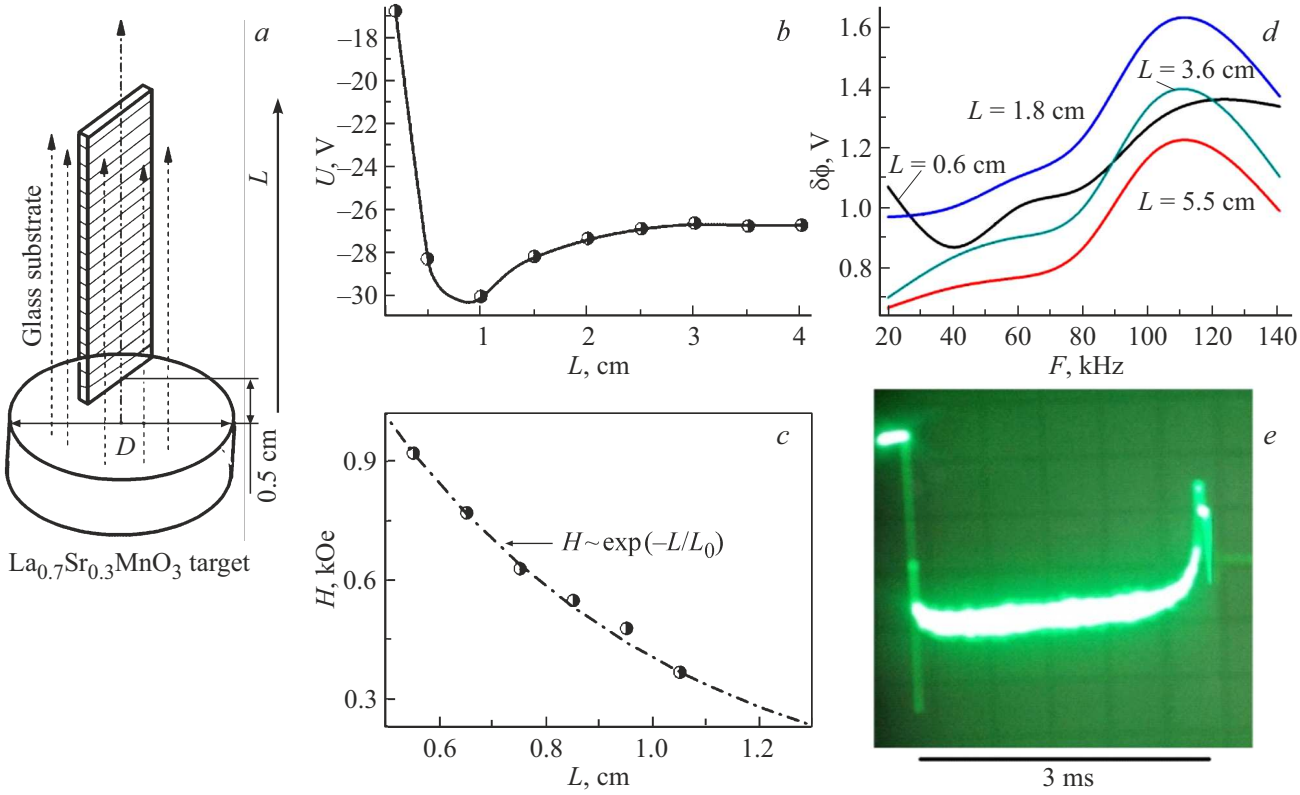

Figure 1. (a) Experimental scheme; dependencies (b) potential and (c) magnetic field on the distance to the target. The measurements were carried out in the deposition zone — along the vertical line passing through the center of the target. (d) — frequency dependences of potential oscillations for four distances from the target; (e) — oscillogram of the voltage pulse on the probe ($L = 2$ cm).

the target. They are best detected in the frequency range of 20–60 kHz (Figure 2, a); wavelengths (distances between neighboring maxima or minima) $\lambda = 0.9$–1.1 cm.

The amplitude of the recorded potential oscillations associated with ionic sound in plasma is small (Figure 2, a). The coefficient of amplitude modulation of the potential by an ion-sound wave $\eta = (\delta\phi_{\max} - \delta\phi_{\min})/(\delta\phi_{\max} + \delta\phi_{\min})$, measured in the target sputtering mode, against the background of an increasing average potential as it approaches the target, is within 1–2%, reaching 10–12% only in the vicinity of the target at a frequency of 20 kHz (Figure 2, a), which indicates a small number of particles involved in harmonic ion-sound vibrations. Noise fluctuations make the main contribution to the total potential at all studied frequencies. In this case, we can talk about the presence in the plasma of a set of ionic components with different masses and charges embedded in a moving stream and moving with it. The distances between the interacting particles involved in the oscillations of a certain frequency should be much smaller than the wavelength. However, incipient oscillations generally have a short propagation length and quickly decay without encountering a suitable medium for them (with similar masses and charges) and are in fact the main sources of noise. To maintain vibrations, it is necessary to have sufficiently extended (at least a wavelength in size) sections containing particles of similar mass and charge state. This requirement imposes strict restrictions on the differences between particles in mass and charge, determining the frequency characteristics of the medium. The maximum amplitude of the recorded vibrations near the target indicates a relation to the particles formed during target sputtering (see Figure 2, a at $L = 0.5$–2 cm).

In the frequency dependences of the potential, the most intense, but wide and blurred maximum, the position of which does not depend on the distance to the target, is observed at frequencies 110–120 kHz (Figure 1, d; in Figure 2, b it is not shown). We associate it with the participation of ions of working gases in the oscillatory process. However, the most interesting features, due directly to plasma clustering, are revealed at lower frequencies. Thus, the next maximum, at the frequency $f \approx 60$ kHz, is observed only near the target ($L = 0.6$–1.2 cm), and the most intense maximum is observed at $L = 1.2$ cm (Figure 2, b). Its nature is determined by the participation of individual ions leaving the target. As the distance from the target increases, their concentration decreases and their contribution to the total potential amplitude sharply weakens (Figure 2, b). The most important result is an increase of the amplitude of the signal near the target, at $L = 0.6$–1.2 cm and $f < 40$ kHz. An increase of the amplitude of the signal with a decrease of frequency characterizes the clustering of

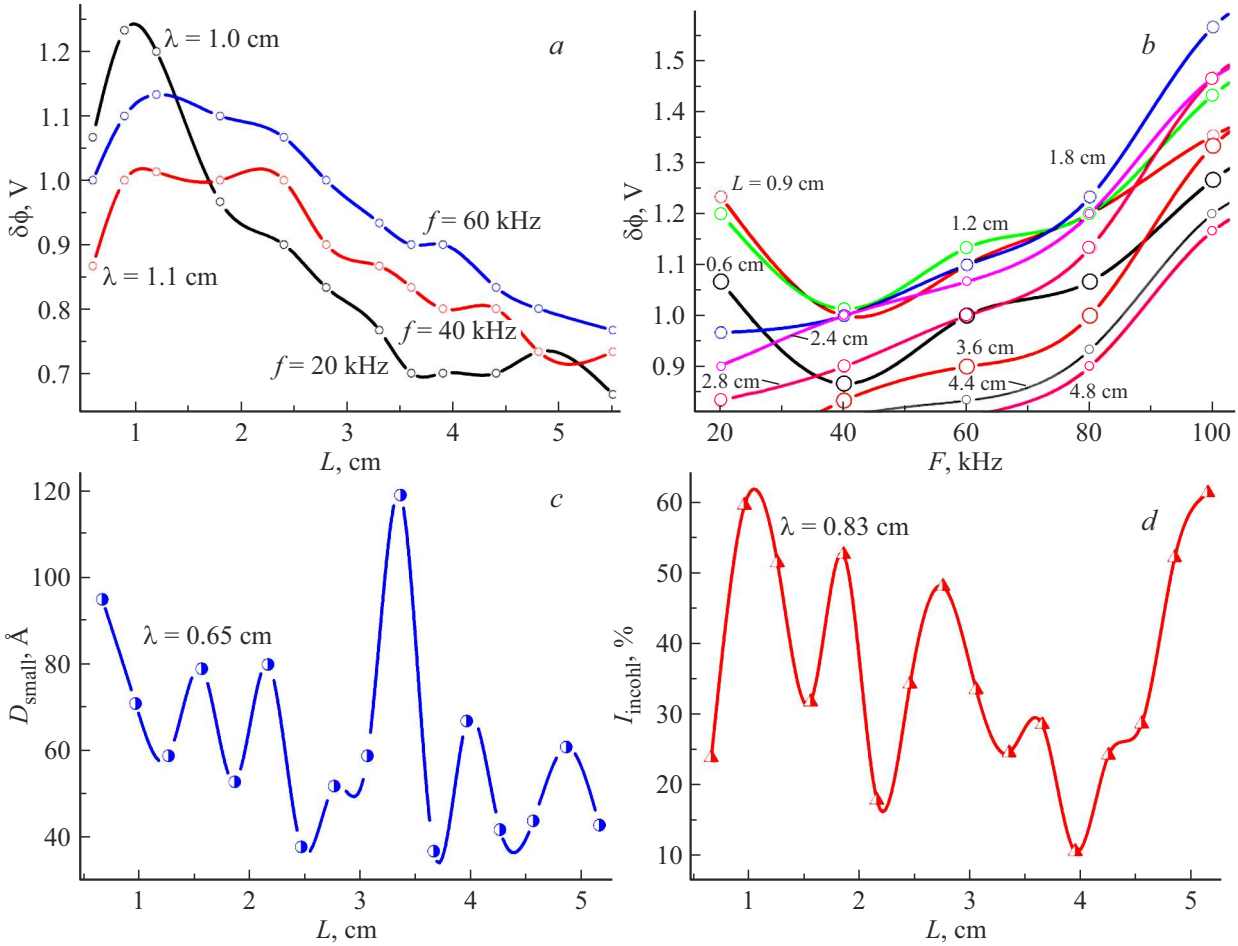

Figure 2. *a*) Spatial potential distributions measured at three frequencies; *b*) frequency dependences of the potential measured at various distances from the target; *c*) size dependencies (D_{small}) of small atomic groupings and *d*) the intensity of incoherent scattering (I_{incoh}) of X-ray radiation from the distance to the target.

the flow associated with the formation of chemical bonds between particles.

The films formed in the magnetron plasma contain ions that are directly involved in ion-sound vibrations in the plasma. „Frozen" oscillations are formed in the deposited films as a result of averaging over a large number of pulses [$(1-2)\cdot 10^6$ imp.] based on harmonics selected from the total number of harmonics involved in the formation of the film structure. At the same time, fluctuations of argon ions, molecular oxygen, etc. are excluded. Therefore, the amplitude of all measurable frozen fluctuations in the film parameters is large, primarily due to averaging the contribution of the same type of vibrations of particles with the same mass and charge. In plasma, during a single pulse, they contribute mainly to noise.

Figure 2, *c* shows changes of the size of small clusters (D_{small}) with a short-range atomic order along the particle flux. Atomic groupings of size D_{small} are clusters of minimal size, which still retain the structural features on a short-range scale characteristic of large clusters $La_{0.7}Sr_{0.3}MnO_{3-x}$, the crystallographic order of which is amenable to structural analysis. The modulation coefficient $\eta_D = (D_{small}^{(max)} - D_{small}^{(min)})/(D_{small}^{(max)} + D_{small}^{(min)})$ „of frozen" oscillations $D_{small} = f(L)$, according to the data in Figure 2, *c*, is many times higher than the corresponding coefficient for real oscillations in plasma (Figure 2, *a*), and varies within 27−72%.

Small clusters of size D_{small} are usually associated with incoherent X-ray scattering I_{incoh} — the most important characteristic of systems with a disordered structure, manifested as a background in X-ray diffraction patterns [7,12]. The value of $I_{incoh} = f(L)$, as well as $D_{small} = f(L)$, periodically changes with distance from the target (Figure 2, *d*). The modulation coefficient $\eta_I = (I_{incoh}^{(max)} - I_{incoh}^{(min)})/(I_{incoh}^{(max)} + I_{incoh}^{(min)})$ „of frozen" oscillations $I_{incoh} = f(L)$ varies from 32 to 52%.

3.2. Film structure

The existence of disordered solid-state systems with only a short atomic order is unlikely, since during their formation, self-organization mechanisms are constantly op-

erating due to the presence of chemical bonding forces and temperatures other than absolute zero [16,17]. As a result, a heterogeneous and, as a rule, highly heterogeneous cluster structure appears in a disordered environment, characterized by the presence of a local order of various scales. Experiments show that in many cases it is possible to put an identity sign between highly disordered and highly heterogeneous systems. It is no coincidence that the model of large-scale potential fluctuations is still the most successful model of the electronic structure of amorphous semiconductors [18].

Films deposited on glass substrates are characterized by a well-developed cluster structure formed by three types of heterogeneous atomic groupings. In X-ray diffraction patterns, coherent radiation scattering is represented by diffuse maxima above the halo with the participation of large clusters of size $D = 150-400$ Å, and halos formed by scattering by smaller clusters ($D = 80-150$ Å). Incoherent scattering involving atomic groupings of size $D = 20-80$ Å forms the background on X-ray pictures (Figure 3, *a, b, c*). The transition from the halo to the background is realized at $D \sim 100$ Å, which corresponds to the maximum length of tunneling in a solid, making it possible to transition in the description of the electronic structure of such samples to a model of large-scale potential fluctuations.

These features are preserved over a wide range of distances from the target. At the same time, the intensity of halos and diffuse maxima, their half-width, which characterizes the cluster sizes, and the background intensity, which is related to the volume and defectness of regions with disordered structure, which partially include the peripheral areas of the clusters themselves, change. Large clusters characterized by a large number of diffuse maxima (up to 25 types), indicating an emerging long-range order, should logically be called crystal clusters [7]. They determine the scale of the intermediate (between short-range and long-range) order. The main difference between such atomic groupings and crystallites is attributable to the presence of peripheral regions comparable in volume to the central parts of clusters, with a smooth transition from order in the central parts to disorder in a disordered intercluster medium. Their formation is directly related to the mechanisms of cluster growth [7,8,19]. Peripheral areas where the maximum defect concentration is realized [20], play a significant role in the structure and properties of clusters [8,12,13,19] and are well detected in magnetic measurements when the atomic [21] or magnetic [19] order is rearranged.

As long as the particles are affected by the electric and magnetic fields of the magnetron ($L < 2.15$ cm), which preserve the stoichiometry of the samples, large clusters form, many of which, even with extended peripheral regions, have a three-dimensional atomic order. Spherical fractal structures each containing up to 10^6 clusters are formed (Figure 3, *d*) near the target ($L < 1$ cm), where the concentration of particles is high. The interfractal medium (not shown; it is similar to the one shown in Figure 3, *f*) is represented by a columnar structure. The following Figure 3, *e* shows a clear tendency of individual fragments to take a spherical shape when they interact on the substrate during growth at the second stage of film clustering. Having a large volume of nanovoids, they possess unusual magnetic properties [8] and are interesting for studying magnetic frustration and mesoscopic phenomena in manganites [19].

At $L > 1$ cm, where the intrinsic magnetic field of the magnetron is small and conditions arise in the plasma for the interaction of ions with electrons and reactions

$$Mn^{4+} + e^- \Rightarrow Mn^{3+} + e^- \Rightarrow Mn^{2+}, \qquad (1)$$

an increase of sample defects is observed which is manifested in an increase of the background I_{incoh} (compare Figure 3, *a* and 3, *b*). The growth of fractal structures ends with a decrease of the concentration of particles along the stream, and only their individual fragments are visible against the background of the columnar structure (see a light spherical object in the upper-left corner of Figure 3, *f* ($L = 1.25$ cm).

The rate of reaction (1) accelerates at $L > 2.1$ cm. Measurements have shown that the concentration of ions Mn^{4+} decreases by 3 times with an increase of L from 1 to 4 cm. As the sample defects increase, intense diffuse maxima are observed in diffraction patterns, which are formed with the participation of fragments of planes including Mn^{2+} ions (Figure 3, *c*). At the same time, the columnar structure collapses, and extended regions containing the MnO phase are visible on the surface of the films (Figure 3, *g*).

Due to the presence of Mn^{3+} and Mn^{4+} ions in the flux, the structure and properties of the films are modulated by ion-sound waves that carry away particles along their path. Figure 4, *a* shows the change in the average size of crystal clusters with distance from the target. The dependence $D(L)$ in Figure 4, *a* is represented by „frozen“ oscillations formed as a result of averaging various modes of real oscillations in the plasma with subsequent modification of the atomic order in the film at the second stage of cluster growth.

3.3. Particle levitation in plasma and cluster structure of deposited films

The formation of the cluster structure of the films occurs due to the partial self-organization of two disordered media of plasma and a growing layer of LaSrMnO. However, if its mechanisms are clear in LaSrMnO (this requires the presence of chemical bonding forces and a temperature other than absolute zero), then these conditions are clearly insufficient for plasma self-organization and clustering. The total particle path does not exceed 8 cm in the pulsed target sputtering mode, but during the pulse time ($\tau \sim 3$ ms), the particle flux, if it continued to exist, could travel an order of magnitude greater distance [7]. It turned out that the activation of the discharge and the sputtering cycle of the target are independent for each pulse, and the average

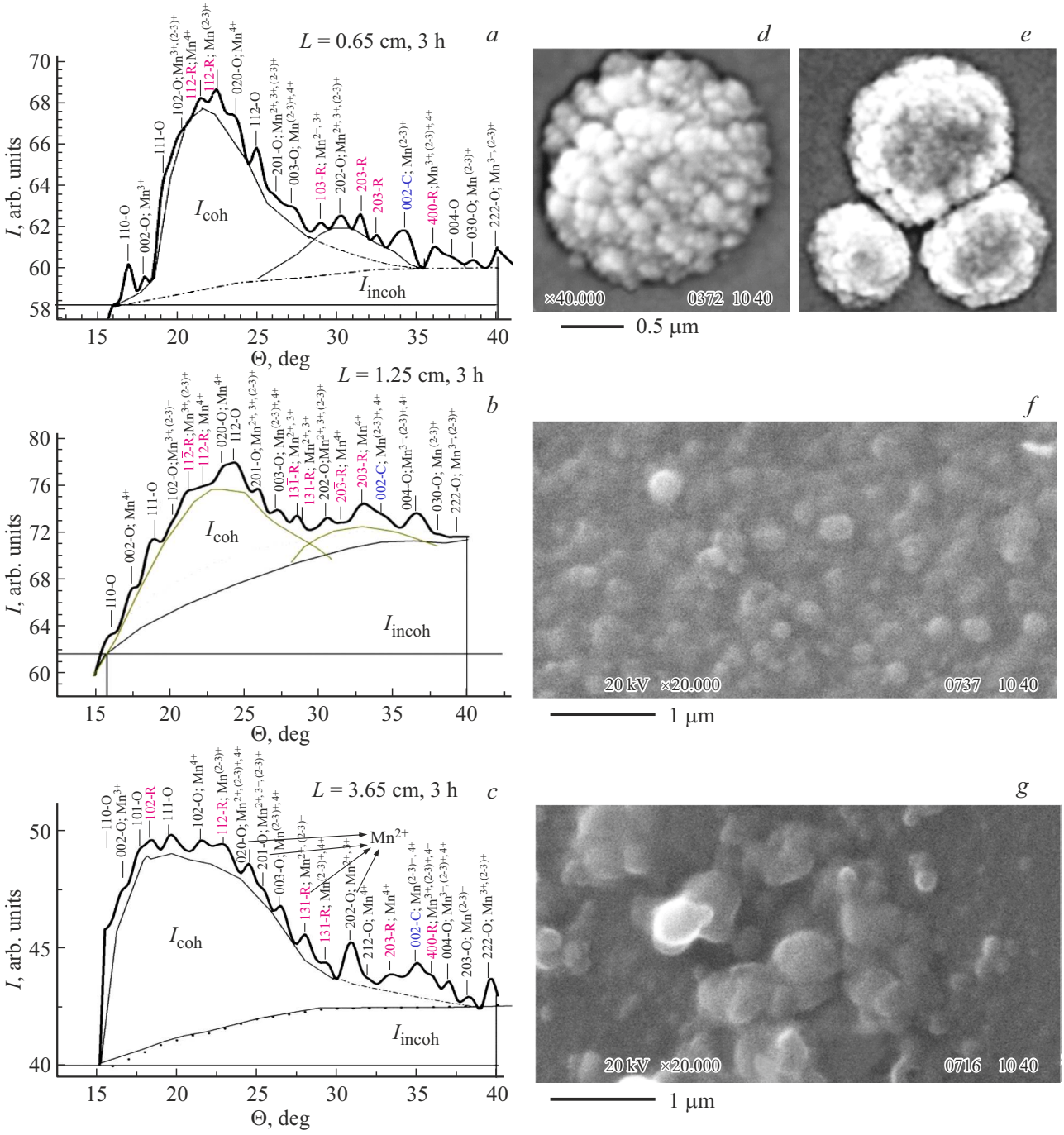

Figure 3. X-ray diffraction pictures and surface images of samples in a scanning electron microscope.

film thickness increases per pulse by an unacceptably small amount — by no more than 0.03 Å. The participation of a large number of pulses in the deposition process is necessary for the formation of a continuous film or the formation of atomic groupings in plasma that would characterize the main features of the structure of the studied manganite.

An analysis of experimental data related to the deposition and development of fractal structures [7,8] has shown that sufficiently large atomic groups and even accumulations of clusters are deposited on the substrate in some cases (see Figure 3, *e*), which is impossible without particle levitation allowing them to be held in free hover mode between the target and the substrate during a large number of pulses. The dependence of the size of crystal clusters on the distance to the target $D(L)$ in Figure 4, *a*, demonstrating a sharp decrease (by half) of the cluster size with a change of L from 2.15 to 2.45 cm is an important argument in favor of the participation of levitation in the formation of the film structure in addition to the obvious evidence of the possibil-

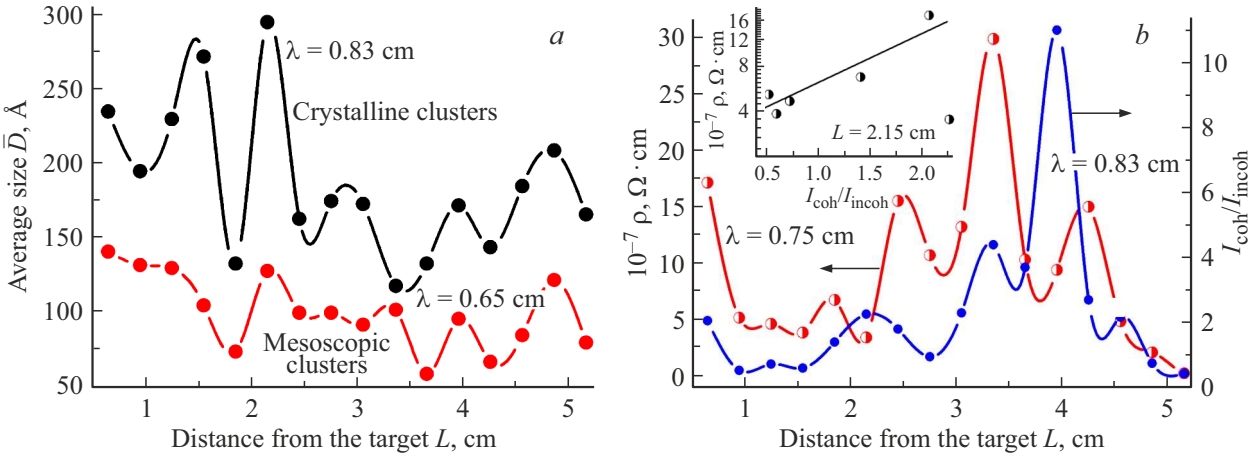

Figure 4. *a*) Change of the cluster size for crystalline and mesoscopic clusters. *b*) The dependence of the resistivity (ρ) of the samples and the parameter I_{coh}/I_{incoh} on the distance to the target; the inset shows the relationship between ρ and the parameter I_{coh}/I_{incoh} for the first 6 points.

ity of deposition of large fragments of fractal structures on the substrate in Figure 3, *e*. The clusters were represented in the form of a disk in the calculations with a diameter of D and a thickness of $D/3$ [12,13,22]. Such changes $D(L)$ are not possible after deposition of the sputtered material on the substrate under the same growth conditions in this range L — in neighboring small areas, several times smaller than the wavelength of ion-sound vibrations, and occur just where the electrical field decreases to small ($E < 1$ V/cm) values (Figure 1, *b*). The changes of $D(L)$ are not so significant for mesoscopic clusters that form halos on X-ray images (Figure 4, *a*); their size is smaller than the size of crystal clusters, and, accordingly, the average wavelength of „frozen" oscillations is smaller. The difference of size for the regions $L \leq 2.15$ cm and $L \geq 2.45$ cm is even smaller for very small groupings represented by the background in diffraction pictures (Figure 2, *c*). Attention should be paid to the behavior of $D(L)$ at one of the special points, $L = 3.35$ cm, at which the maximum resistivity (ρ) of samples is observed over the entire length of the particle path from the target (Figure 4, *b*). The studied samples still retain a single-phase state at $L \leq 3.35$ cm despite a noticeable decrease of the ion concentration Mn^{4+} (the main reason for the increase ρ). This unusual disordered state before the phase transition is characterized by the proximity of the cluster size (within 100–115 Å) for all three structural fractions. The samples become two-phase with a further increase of L and the formation of inclusions of the green phase of MnO.

Ion-sound waves are another significant factor influencing particle levitation. A direct confirmation of their participation in levitation is the modulation of the cluster size in Figure 4, *a*. And if the modulation of the properties of samples within some limited ranges of L can be explained by the participation of individual ions (or the simplest charged complexes consisting of a small number of atoms), then any modulation of the size of large clusters is not possible in a film already forming on a substrate under the impact of ionic sound. Ionic sound participates in levitation along the entire length of the particle path, while the electric field is only in the first third of the path. In accordance with our study, ionic sound is represented by numerous harmonics, which are determined by the size and charge state of atomic groupings. All of them contribute to the ionic sound pressure. However, levitation will obviously involve only ion-sound oscillations that are close in phase.

The internal fields of the magnetron play a significant role in the formation of the structure of films, exerting a decisive influence on their properties. The magnetic field removes electrons from the space near the target, preventing the occurrence of reaction (1) and contributing to the preservation of the stoichiometric composition of the films. The electric field plays an important role in the formation and growth of clusters in plasma. Three forces act on a particle moving away from the target: electrostatic

$$F_e(L) = Z_d(L)eE_{eff}(L), \text{ where } E_{eff} = \left[1 + \frac{(a/\lambda_D)^2}{3(1 + a/\lambda_D)}\right],$$

a is its radius, λ_D is the Debye screening length in plasma and E is the electric field [3]; gravitational $F_g = m_{cl}g$, where g is the acceleration of gravity, m_{cl} is the mass of the particle; and the force of particle entrainment by ionic sound (F_l). For sine waves $F_l = \sum_j \chi_{j0}(Z_d, m) \cdot \sin[\omega_j(Z_d, m)t + \varphi_j]$, where χ_{j0} is the amplitude of the jth mode of oscillation, ω_j is the frequency and t is the time. Forces $F_e + F_l$ and F_g balance each other at rest for $L \leq 2.15$ cm, and then it is possible to write

$$Z_d eE_{eff}(L) + \sum_j \chi_{j0}(Z_d, m) \cdot \sin[\omega_j(Z_d, m)t + \varphi_j]$$

$$= m_{cl}g = p \cdot 1/6\pi \cdot D^3 g, \quad (2)$$

where χ_{j0} is the amplitude of the jth component of the wave and p is the density. For the space $L \geq 2.45$ cm, in

which only the force associated with ion-sound pressure acts, we have

$$\sum_j \chi_{j0}(Z_d, m) \cdot \sin[\omega_j(Z_d, m)t + \varphi_j] = p \cdot 1/6\pi \cdot D^3 g \quad (3)$$

The impact of F_l can be taken into account using the experimental dependence $D(L)$ for crystal clusters in Figure 4, *a* for quantitative estimates, due to the difficulties of calculating F_l for such a complex system. All three forces act on particles (F_e, F_l and F_g) in the first third of the particle path ($L \leq 2.15$ cm), and only two forces such as F_l and F_g act on the particles at $L \geq 2.45$ cm which reduces the cluster size by half. Thus, given the ratio (2), the size of the clusters for $L \leq 2.15$ cm is

$$D(L \leq 2.15\,\text{cm}) = \left\{ 6\pi \frac{Z_d e E_{eff}(L) + \sum_j \chi_{j0}(Z_d, m) \cdot \sin[\omega_j(Z_d, m)t + \varphi]}{pg} \right\}^{1/3}$$

$$= \left\{ 6\pi \frac{F_e + F_l}{pg} \right\}^{1/3} \quad (4)$$

The particles levitate out only due to the pressure of ionic sound with distance from the target ($L \geq 2.45$ cm), and then

$$D(L \geq 2.45\,\text{cm}) = \left\{ 6\pi \frac{\sum_j \chi_{j0}(Z_d, m) \cdot \sin[\omega_j(Z_d, m)t + \varphi]}{pg} \right\}^{1/3}$$

$$= \left\{ 6\pi \frac{F_l}{pg} \right\}^{1/3}. \quad (5)$$

The approximate equality $D(L \leq 2.15\,\text{cm}) \approx 2D(L \geq 2.45\,\text{cm})$ can be written in accordance with the data in Figure 4, *a* for assessment of the ability of the forces F_e and F_l to influence particle levitation, according to which, using (4) and (5), it has a simple form:

$$\left\{ 6\pi \frac{F_e + F_l}{pg} \right\}^{1/3} \approx 2 \left\{ 6\pi \frac{F_l}{pg} \right\}^{1/3}, \quad (6)$$

where the following is obtained

$$F_e + F_l \approx 8F_l \quad (7)$$

It can be seen from the ratio (7) that the contribution of F_l to particle levitation at $L \leq 2.15$ cm is about 12%. Judging by the change of the amplitude of „frozen" fluctuations of the average cluster size in Figure 4, *a*, this ratio between F_e and F_l changes little in this range of variation of L: apparently, the decrease of the number of particles in the flux, accompanied by a decrease of the ion-sound pressure with distance from the target, is largely compensated by the attenuation of the electric field (Figure 1, *b*). Thus, during particle levitation — from individual ions to large charged groupings of clusters up to 10^4 angstroms — electric fields are more effective for increasing the size of atomic groupings compared to the entrainment of particles by ion-sound waves. At the same time, the force of particle entrainment by ionic sound (ion-sound pressure) is the only force ensuring the plasma clusterization at $L \geq 2.45$ cm.

Two regions are identified in Figure 4, *a*: $L \leq 2.15$ cm and $L \geq 2.45$ cm. A tendency for the increase of the size of clusters with L is observed in both regions: a decrease of the energy of particles, even with a significant decrease of their concentration in the flux, leads to an increase of the probability of their chemical interaction and to the growth of clusters to a critical size determined by the ratios (4) — for the region $L \leq 2.15$ cm and (5) — for $L \geq 2.45$ cm.

Negatively charged (at $L > 0.9$ cm) and positively charged (at $L < 0.75$ cm) particles levitate over the target according to Figure 1, *b*, depositing on the substrate upon collision with it. The gravitational force only slightly affects the distance of the particle to the target after the pulse ends due to the smallness of the term $(\delta\tau)^2$:

$$L = L_0 + V_0 \cdot \delta\tau - \frac{g(\delta\tau)^2}{2}, \quad (8)$$

where V_0 is the initial velocity of the particle and $\delta\tau = 4$ ms is the interval between the pulses. The space in which particle levitation can be observed depends on the energy and mass of the particles. This is realized in the range of L from 0.2 to 2.1 cm with the participation of an electric field in accordance with our results. Particles can stay in this space for a long time for a large number of pulses with an increase of their size and improvement of their atomic order.

The levitation is possible with the participation of an electric field for both positively charged (at $L < 0.75$ cm) and negatively charged particles (in the range $L = 0.9-2.15$ cm) according to Figure 1, *b*. The change of the sign of the particle charge is possible in the small range of variation $L = 0.75-0.9$ cm, where the derivative is $dU/dL \approx 0$, i.e their recharge. There is a maximum size (D_{crit}) of atomic groupings for each value of L that can be in a state of levitation. The required number of pulses is determined by the value D_{crit} and depends on the concentration of particles and their charge in the flow. The size of levitating atomic groupings is $D_{crit} = 0.13\,\mu$m according to the formula (4), for $Z = 1$ and $L = 0.95-1.25$ cm in the region $L \leq 2.15$ cm, if we do not take into account the small contribution of ion-sound waves to particle levitation. The light spherical fragment of the fractal structure in Figure 3, *f* is formed at $Z \approx 16$. D_{crit} decreases to $0.075\,\mu$m with distance from the target at a distance of $L = 2.15$ cm. The value of D_{crit} is higher for positively charged particles: the size is $D_{crit} = 0.19\,\mu$m in the vicinity of $L = 0.5$ cm. This is consistent with the data in Figure 3, *e* for $Z \approx 60-300$.

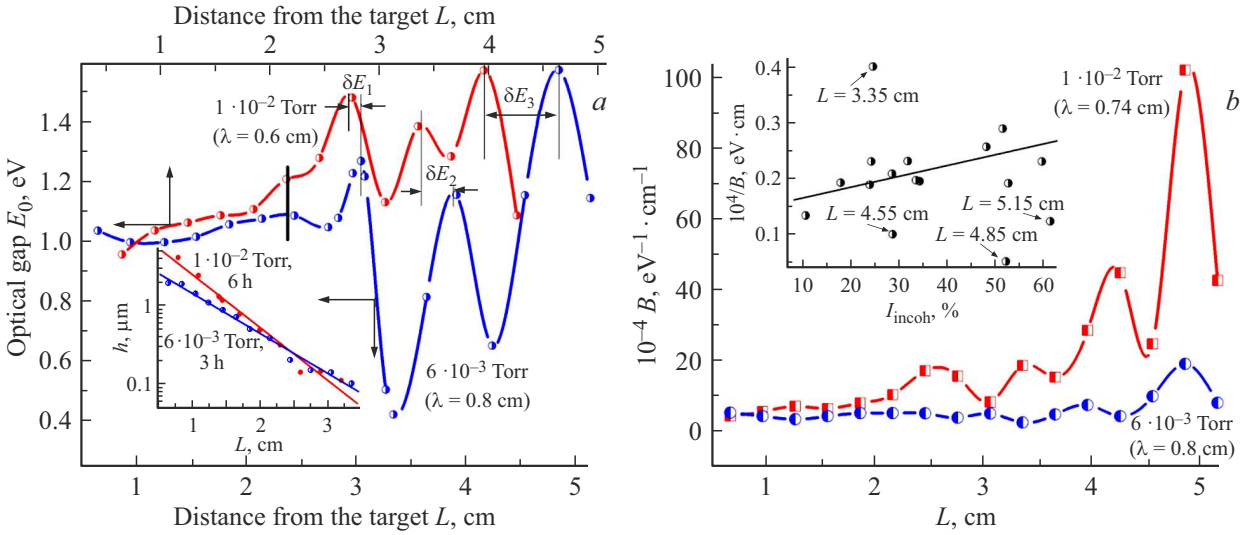

Figure 5. *a*) The dependence of the effective optical band gap of the studied samples on the distance to the target (L) for two working gas pressures; the insert shows the dependence of the thickness of these samples on the distance to the target; 6h — film growth over 6 hours and 3h — 3 hourly growth. *b*) Parameter change B with the distance from the target for two working gas pressures — $6 \cdot 10^{-3}$ Torr (film growth during 3 hours) and $1 \cdot 10^{-2}$ Torr (film growth during 6 hours). The inset shows the relationship between the parameters B and I_{incoh}.

The critical region in the vicinity of $L \sim 2.15$ cm is also revealed in the behavior of the resistivity (ρ) and the parameter I_{coh}/I_{incoh} (insert to Figure 4, *b*).

Ion-sound oscillations modulate the influx of particles onto the substrate without affecting the growth of the film after deposition on the glass, providing a direct link between plasma phenomena, the structure and properties of the film. As a result, all the parameters of the samples represent „frozen“ fluctuations, the real characteristics of which were observed in plasma. Experiments have shown that the frequency of „frozen“ fluctuations in films, as well as the frequency of ion-sound oscillations in plasma, depends on the pressure of the working gas.

3.4. Ion-sound vibrations and optical properties of films

Figure 5 shows the dependences of the effective optical band gap (E_0) of the studied samples on the distance to the target for two working gas pressures. The value E_0 was determined using the Tauc ratio [23], which is universal for amorphous semiconductors

$$\alpha = B\frac{(\hbar\omega - E_0)^2}{\hbar\omega} \tag{9a}$$

$$B = \frac{4\pi\sigma_{\min}}{nC\delta E}, \tag{9b}$$

where α is the absorption coefficient, E_0 is the optical band gap, $\sigma_{\min}$ is the minimum metallic conductivity, δE is the band width of localized states and C is the speed of light. Periodic changes of E_0 from L are observed. It can be seen from the figure that both curves are qualitatively similar, and their main changes are associated with a decrease of the amplitude and wavelength of „frozen“ fluctuations from 0.83 cm to 0.6 cm with the increase of pressure in the chamber. For greater clarity, the curves are shifted relative to each other by 0.22 cm — so that the first clearly visible and closest maxima to the target (indicated in the figure by a vertical bold line) coincide; to ensure the same scale, the axis lengths are L (4.7 cm) in both cases, they were equal. It is clearly seen that the distance between such maxima increases from L: $\delta E_1 < \delta E_2 < \delta E_3$, characterizing the decrease of wavelength with increasing pressure in the chamber.

The gap E_0 increases with the increase of the growth time: an increase of the size of atomic groupings leads to a decrease of the tails of the density of states and the expected growth of E_0 for samples grown for 6 hours. It could be assumed based on the presented data that diffusive blurring of heterogeneities takes place in plasma with the increase of deposition time when the particle flux is modulated by an ion-sound wave, which eliminates spatial differences in the local atomic order and properties of samples, weakening the memory of plasma clustering processes, and is a clear example of changes of structure and properties of samples at the second stage of clustering. This mechanism involves an increase of the temperature of the substrate due to radiant heating from a heated target and thermalization of particles deposited on the substrate. If the heat sink is not efficient enough, the longer the growth time, the higher the temperature, and this should be most pronounced near the target, however, as can be seen from Figure 5, *a*, in the range $L \leq 2.15$ cm values E_0 for 3 and 6 hours are almost the same, and, therefore, the nature of the effect of growth time on E_0 is other.

Figure 5, *b* shows the changes of the parameter B in the Tauc formula (9), which, when the values $\sigma_{\min}$ and n are constant, is inversely proportional to the width of the zone of localized states involved in optical transitions. Attention should be paid to the enormous effect of growth time on the value of B for samples $L > 2.15$ cm. This is in good agreement with the behavior of the optical band gap E_0 in Figure 5, *a*. The absence of the same effect on both parameters of the samples falling into the range of $L \leq 2.15$ cm, where an increase of their temperature is possible (no higher than 150°C under experimental conditions), shows that a significant decrease of the value of δE and the increase of E_0 with the increase of the growth time is not related to heating of the samples and is most likely attributable to particle levitation depending on the time of growth of the films. Figure 5 also shows that the parameters E_0 and δE do not depend on the growth time at 3 and 6 hours in case of the participation of magnetron electric fields in levitation and the formation of atomic groupings in plasma. This means that the critical (maximum) formation times of atomic groupings during levitation under the impact of electric fields are less than 3 hours. At the same time, the critical particle formation times exceed 6 hours at $L > 2.15$ cm, where ion-sound waves remain the only mechanism of particle levitation, which have a significantly lower impact on the levitation compared to electric fields, and the parameters E_0 and δE strongly depend on the growth time.

The data presented in Figures 5, *a* and 5, *b* are a clear illustration of the participation of ion-sound waves in particle levitation. Their participation in levitation and film structure formation is minimal at $L \leq 2.15$ cm, and therefore „frozen" fluctuations are practically not detected on the dependences $E_0 = f(L)$ and $B = f(L)$. At the same time, in the region of $L \geq 2.45$ cm, in which ion-sound waves play a major role in particle levitation, in the formation, development, and modulation of the flux before deposition on a substrate, „frozen" fluctuations of film parameters turn out to be very expressive.

A study of the possible relationship between the width of the zone of localized states δE, determined by the parameter B, and the intensity of incoherent X-ray scattering (I_{incoh}) yielded a positive result (see inset in Figure 5,*b*), which indicates a direct dependence of the value δE on the structural disorder.

3.5. Charge states of manganese ions, particle levitation in plasma, and special states in the cluster structure of films deposited along the particle flux

Conditions for the growth of films with a wide variety of structures and properties of samples are created under the impact of the internal fields of the magnetron, with changes of the concentration and energy of levitating particles in the flux. Fractal structures (Figure 3, *d*) where clusters possess metallic conductivity and ferromagnetism can grow in the immediate vicinity of the target ($L < 1$ cm), where the magnetic field (Figure 1, *c*) limits the effect of reaction (1) on the composition of the particle flux and contributes to the preservation of the stoichiometric composition of the samples [7,8]. The ion concentration Mn^{4+} markedly decreases in the range $1 \leq L \leq 2.15$ cm with a loss of ferromagnetism [19]. The levitation mode of particles changes at $L > 2.15$ cm when electric fields cease to act, which qualitatively changes the relationship between electrical conductivity and the parameter I_{coh}/I_{incoh}. A further decrease of the concentration of Mn^{4+} ions takes place, accompanied by an increase of structural disorder and an increase of the difference from the state of the samples deposited near the target, but the basic features of their structure is still preserved. This interval is closed by the sample $L = 3.35$ cm with the maximum resistivity (Figure 4, *b*).

16 experimental points characterize the relationship between the width of the localized state zone and the intensity of incoherent scattering in the insert to Figure 5 and only 4 of them clearly fall out of the presented dependence. Moreover, 3 of them can be attributed to large errors of determination of the parameters of small-thickness film samples ($d \leq 200$ Å at $L \geq 4.55$ cm). And only one point ($L = 3.35$ cm), being critical in the behavior of many film parameters, is of interest for discussion. An approximate equality of atomic group sizes is observed for all three types of structural fractions at this point with an unusual combination of the minimum optical gap (Figure 5, *a*) and the maximum resistivity of the samples (Figure 4, *b*), (Figure 2, *a*, 4, *a*). The high resistivity is apparently related to the low density of states involved in hopping conduction. A significant increase of δE and a significant narrowing of the gap E_0 are possible with a significant disordering of the sample structure. Such a strong disordering, as measurements have shown, occurs with a change of the ratio between the concentrations of Mn^{3+} and Mn^{4+} ions (it was determined using X-ray spectral measurements of strontium concentration), which changes by more than 2 times in favor of Mn^{3+} ions due to the reaction (1) and the index characterizing the concentration of strontium in film samples in the chemical formula $La_{0.7}Sr_{0.3}MnO_3$ obviously reaches a critical value of 0.15 instead of 0.3, at which the transition of samples takes place from rhombohedral into the orthorhombic structure characteristic of the undoped $LaMnO_3$ [24], which is the reason for the strong disordering.

The heterogeneity of the samples increases in the interval $3.35 < L \leq 3.95$ cm and a two-phase state is initiated. All three structural fractions considered in the study are interdependent and interact with each other. The largest influence on the structure of samples and the density of localized states is exerted by large (crystalline) clusters (Figure 6, *a*). It can be seen from this figure that there are 2 areas of change in the ratio I_{coh}/I_{incoh}. Localized states in films, as schematically shown in a simple two-dimensional cluster model in the insert to Figure 6, it a, are concentrated mainly in the peripheral regions of clusters, and therefore, assuming

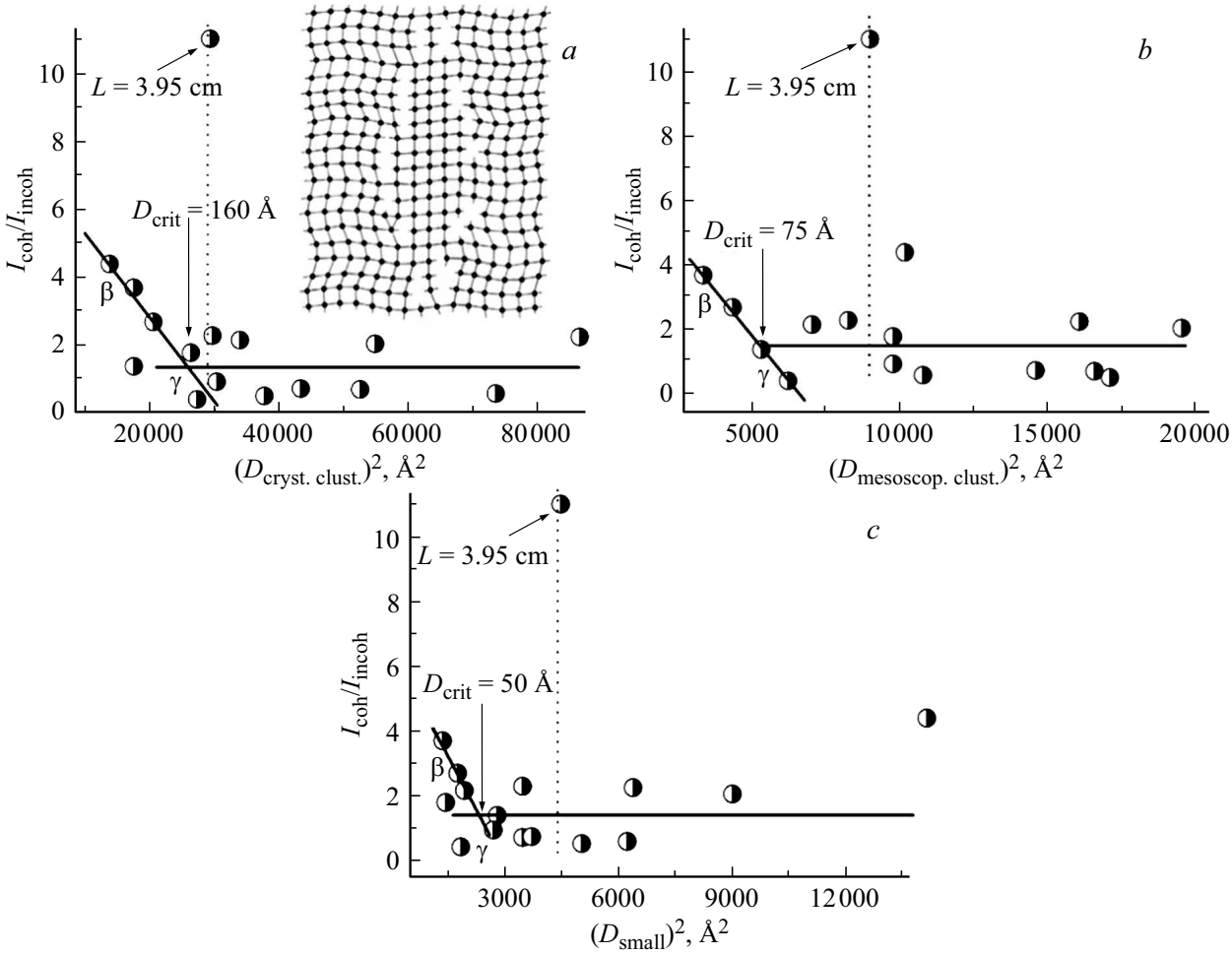

Figure 6. Relationship of the parameter I_{coh}/I_{incoh} with the sizes of crystalline (a), mesoscopic (b) and small (c) clusters.

there is a relation between I_{incoh} and structural defects, we look for dependencies of the parameter I_{coh}/I_{incoh} on the cluster surface area proportional to D^2. Initially, a noticeable decrease (by 4–4.5 times) of the value of I_{coh}/I_{incoh} is observed with an increase of D^2 (Figure 6, a), and then it doesn't change anymore in a wide range of D^2. Apparently, the surface density of defects decreases because of the limitations associated with the amount of free energy, which, if not limited to its growth, calls into question the very existence of large clusters with a developed surface in a disordered medium. For mesoscopic clusters and small atomic groupings, the bonds of I_{coh}/I_{incoh} with D are qualitatively similar (Figure 6, b and 6, c), but less pronounced and accompanied by a large spread of experimental points. The critical cluster size, above which I_{coh}/I_{incoh} does not depend on D, decreases from 160 Å for crystal clusters to 50 Å for small clusters.

There is a point $L = 3.95$ cm in Figure 6, for all three structural fractions, where a significant change (by 7 times) of the parameter I_{coh}/I_{incoh} is observed. The revealed ordering of the cluster structure is accompanied by a sharp increase of the electrical conductivity of the samples (Figure 4, b), which is not characteristic of the amorphous state of these films [7]. In this case, the only possible cause of the observed changes may be the formation of inclusions of the second phase associated with the action of reaction (1), which is realized beyond the impact of the electric and magnetic fields of the magnetron, and the appearance of the MnO phase in significant quantities (in the presence of Mn^{2+} ions), which should not be present in the material of this composition. Its electrical conductivity is higher compared to the base structure [25]. MnO phase in the sample $L = 3.95$ cm (because of the color of the crystals, it is called the green phase [25]) is detected in the reflection spectrum [7]. The refractive index spectrum obtained on their basis, in addition to the main maximum, contains an additional maximum at higher quantum energies that actually corresponds to the green color in the optical spectrum, which is limited by two vertical dotted lines in Figure 7, a.

The presence of atomic groupings with a predominance of Mn^{2+}-O bonds, the parameters of which correspond to the green region of the spectrum, is confirmed by a detailed study of absorption spectra. The Tauc ratio (9a) can be

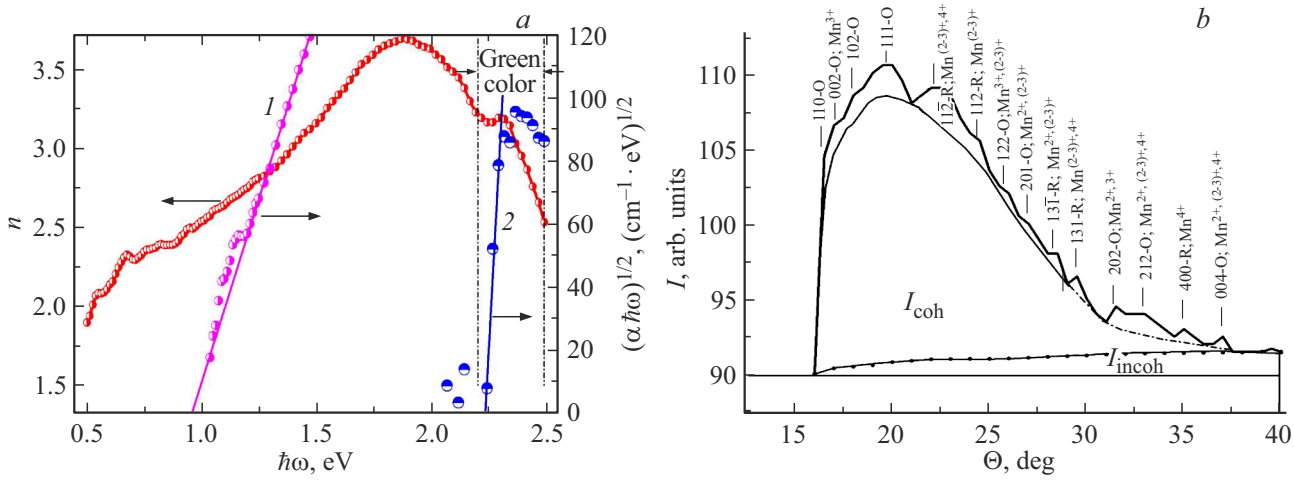

Figure 7. *a*) Refractive index and optical absorption spectra in Tauc coordinates $(\alpha\hbar\omega)^{1/2} - \hbar\omega$ and *b*) diffraction pattern of the sample $L = 3.95$ cm.

rewritten as follows for a two-phase system in accordance with the rule of additivity of absorption coefficients [26]

$$\alpha_{Full} = (1 - C_{MnO})\alpha_{LSMO} + C_{MnO}\alpha_{MnO}$$
$$= B_{LSMO}(1 - C_{MnO})\frac{(\hbar\omega - E_0^{LSMO})^2}{\hbar\omega}$$
$$+ B_{MnO}C_{MnO}\frac{(\hbar\omega - E_0^{MnO})^2}{\hbar\omega} \qquad (10)$$

where the LSMO and MnO indices refer to the main matrix phase and to inclusions of the MnO phase, respectively, and C_{MnO} is the concentration of MnO. Two conditions should be fulfilled to obtain the absorption spectrum of MnO with the simplest subtraction procedure using (10): 1) the spectra of both phases can be approximated by the Tauc ratio (9a) and 2) in the region of small $\hbar\omega$, the possible contribution of MnO to the total absorption spectrum can be neglected. Both of these conditions are fulfilled. It can be seen from Figure 7, *a* that the absorption edge of the second phase is in the green region of the spectrum and corresponds to the spectrum of $n(\hbar\omega)$.

The MnO phase does not occur immediately. Initially, Mn^{2+} ions, forming part of the film, form Mn^{2+}-O bonds. If they are directly adjacent to Mn^{3+} ions, which, according to the reaction (1), are already very numerous at high L, then, for reasons of local electroneutrality, there is a high probability of an electron transition from the Mn^{3+} ion to the nearest oxygen ion with the formation of Mn^{4+} ion. Thus, the adjacency of Mn^{2+}, Mn^{3+}, and Mn^{4+} ions can be observed without the formation of a second phase, which occurs with an increase of local stresses with large amounts of Mn^{2+} ions in the film. The sample $L = 3.95$ cm represents this critical condition. Reflections of the orthorhombic phase are observed in its diffraction pattern along with reflections of the main rhombohedral phase (Figure 7, *b*), which indicate violations of the lengths of interatomic bonds because of the presence of charged states of manganese, which are sources of local stresses in the structure of the samples. As a result, Mn-O bonds with a constantly changing set of charge states are formed by manganese ions in manganite B-sublattice under the action of reaction (1) with increase of the distance from the target: Mn^{2+}, $Mn^{(2-3)+}$, Mn^{3+} and Mn^{4+}. Inclusions of the MnO phase begin to form with $L > 3.95$ cm.

The intensity of the second halo is low in the diffraction picture of the sample $L = 3.95$ cm (Figure 7, *b*), and its contours are weakly pronounced against the background of the tail of the main diffraction maximum of the first halo, which indicates a low concentration of Mn-containing ion groupings in the B-sublattice of manganite. The electrical conductivity increases (Figure 4, *b*) because of the shunting of the main dielectric matrix by groupings with Mn-O bonds with higher electrical conductivity [25]. A comparison of the behavior of curves I_{coh}/I_{incoh} and ρ in Figure 4, *b* shows that changes of the electronic structure outpace changes of the atomic order. The sample $L = 3.95$ cm is characterized by a large number of planes with mixed charge states with the dominance of Mn^{2+} ions in the structure. The very weak background compared to the surrounding samples confirms the presence of a highly ordered state with a low concentration of defects, thus resembling the effects observed in case of structural resonances in multicomponent amorphous alloys [16].

3.6. Electrical conductivity of a multi-dimensional cluster structure and the Lifshitz model

The electrical conductivity (σ) of the studied samples is 8–10 orders of magnitude less than the minimum of metallic conductivity, and the main mechanism of their conductivity is the hopping conduction [22], depending on the concentration of Mn^{3+} and Mn^{4+} ions and on the overlap of the associated localized states [7]. Other

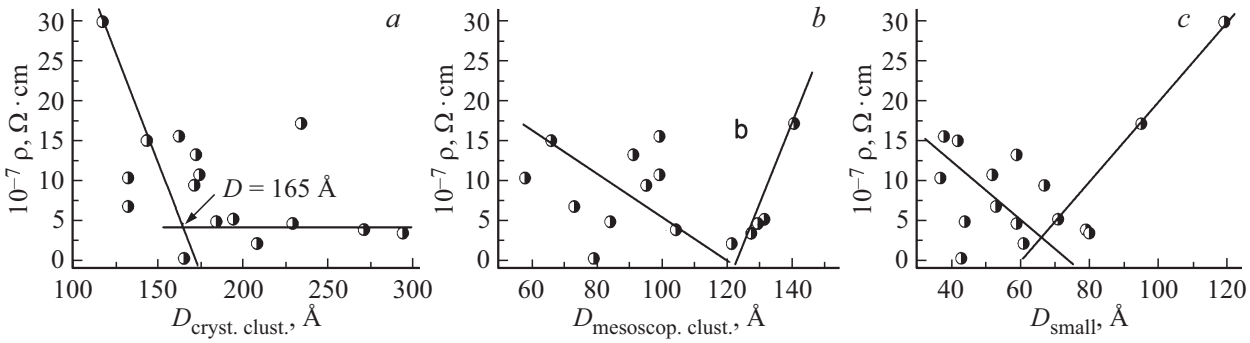

Figure 8. The relationship between the resistivity of samples and the cluster sizes for different structural groups.

types of tunnel transitions can also be realized, but in the presence of local metallic conductivity, which was observed in the optical spectra of samples containing clusters with the size of at least 350 Å [7]. Mn^{3+} and Mn^{4+} ions in the clusters participate in conductivity separately in all cases. However, collective phenomena still affect the value of σ due to the reduction (in the presence of ferromagnetic interactions involved in this material at $T < 350$ K) or increase (if there is local antiferromagnetism) of the activation energy of hopping conduction [22,27]. This is essential at low temperatures for the electrical conductivity of nanostructures, which include the studied samples with large clusters [13,19,28].

The state of the cluster structure plays a key role in the electrical conductivity of the samples. The ratio I_{coh}/I_{incoh} is the most sensitive parameter characterizing it (Figure 4, *b*). This is most clearly manifested in one of the singular points $L = 3.35$ cm (inset in Figure 5, *b*). The relationship of the electrical conductivity of the samples with the cluster sizes is less obvious and is revealed indirectly by the influence of the cluster size D on the parameter I_{coh}/I_{incoh} — because of the change of D in the rangeof $L = 2.15-2.45$ cm in the inset to Figure 4, *b* or in Figure 6 where a special point $L = 3.95$ cm is identified.

The properties of clusters with low concentrations of Mn^{4+} ions insignificantly differ from properties of a disordered intercluster medium, and the potential relief in the samples is created mainly by clusters in which Mn^{4+} ions are present in significant quantities, a significant part of the states of which is localized because of the presence of extended peripheral regions of clusters. The critical size is determined by the Debye screening radius (l_D) and can be comparable to the hopping distance. Since it is known that the metallic conductivity in clusters disappears at $D < 350$ Å [7], it can be confidently stated that the value of $l_D = 175 \mp 30$ Å, which exceeds the maximum tunneling length in a solid — 100–120 Å. The occurrence of embedded electric fields is inevitable with a heterogeneous distribution of Mn^{3+} and Mn^{4+} ions in the peripheral regions of clusters with $D > l_D$. Coulomb blockade is also more pronounced in environments with large clusters in case of a charge transfer [13], which further complicates understanding the experimental results.

A qualitative correspondence in the behavior of the parameter I_{coh}/I_{incoh} and ρ is observed for $L < 2.15$ cm in Figure 4, *b*, which is understandable within the framework of the hopping conduction model, but it is limited to the data for five samples, close to the target (see insert in Figure 4, *b*). There is no similar relationship between I_{coh}/I_{incoh} and ρ in the region of large L in which a sharp decrease of D is observed in Figure 4, it a for crystal clusters. The results related to the effect of cluster size on the electrical properties of the samples turned out to be the most difficult to understand.

The Lifshitz model [29], known as the „model with structural disorder“ [18], is the most acceptable of the well-known models of localization of electronic states (Mott, Anderson, and Lifshitz) that we used to interpret the results. Each cluster containing Mn^{4+} ions has its own quantum well in this case. The dependence of the density of states on the energy $g(\varepsilon)$ is given by the following expression for deep wells [29]

$$g(\varepsilon) \approx \frac{2\pi N^2}{\alpha^3} \frac{[\ln(|\varepsilon|/\lambda\alpha)]^2}{|\varepsilon|}, \qquad (11)$$

where N is the concentration of wells, α^{-1} is the radius of the state and λ is a parameter depending on the asymptotics of the wave functions. In our case, the wells are created in large clusters by the states Mn^{3+} and Mn^{4+}, which occur in manganite doped with strontium due to phase separation. For the case of small ε, characteristic of smaller clusters,

$$g(\varepsilon) \infty \exp\left[-\frac{\pi N}{6\alpha^3}\left(\ln(\varepsilon_0/|\varepsilon|)\right)^3\right]. \qquad (12)$$

We studied the effect of cluster size for all three structural fractions, considering that there is a definite relationship between cluster size and the depth of the quantum well, at least up to sizes less than twice the Debye screening radius. This condition is fulfilled for almost all the studied samples. One would expect that in the presence of metallic conductivity, the depth of the potential well is saturated with D, but this is possible in the presence of clusters with $D > 400$ Å, which are not present in the studied samples.

Figure 8 shows the dependences of the resistivity of the samples on the size of the clusters. The influence of all three types of atomic groupings on the electrical conductivity of the samples is observed. There is no agreement with the Lifshitz model in case of large clusters: the values of ρ do not depend on D after a decrease of resistivity with an increase of cluster size, starting from a value of D corresponding to the Debye screening radius. Apparently, this is associated with an increase of the density of localized states from D, which is not taken into account by the Lifshitz model: the generation of localized states actually suppresses the mechanism proposed by Lifshitz. It should be noted that the intersection point of the segments of two straight lines ($D = 165$ Å) in Figure 8, *a* corresponds to $D_{crit} = 160$ Å in Figure 6, *a*. This result indicates that clusters with a stable structure are formed in the range of $D = 100-160$ Å.

The relationship between the size and electrical conductivity of the samples is in agreement with the Lifshitz model in case of clusters of smaller sizes (Figure 8, *b, c*): areas of decrease of resistance are first observed with small D because of an increase of the density of localized states involved in conductivity with D (see Figure 6, which shows the dependence of the parameter I_{coh}/I_{incoh} on D^2), and then the resistance increases with an increase of D. We attribute the large spread of experimental points in Figure 8 to the active participation of all three structural fractions in the electrical conductivity.

4. Conclusion

By studying the structure and properties of films deposited on glass substrates in a magnetron plasma along the flux of particles produced in case of sputtering of the target $La_{0.7}Sr_{0.3}MnO_{3-x}$, we have shown that particle levitation plays the main role in the formation of atomic groupings in plasma and in the generation of the film cluster structure due to two reasons: the presence of electric fields (only in the first third of the particle path) and the action of ion-sound waves affecting the flux along the entire length of the particle path. The calculated critical sizes of atomic groupings in low-temperature plasma are consistent with experimental values of the sizes of fractal structures on the surface of $La_{0.7}Sr_{0.3}MnO_{3-x}$ films. A quasi-stationary levitating flux arises in the target sputtering operating mode and groupings that do not satisfy the ratios (4) and (5) leave this flux, but it is constantly replenished with particles generated during target sputtering. The charge state of clusters in plasma is a random variable (and here, the magnetic field plays a large role primarily in the vicinity of the target) and it is the main factor determining the features of the local structure and the size of atomic groupings in films. „Frozen“ fluctuations in $La_{0.7}Sr_{0.3}MnO_{3-x}$ films reflect real fluctuations in plasma. The observed dependence of the film parameters on the growth time and pressure in the working chamber is a clear illustration of the processes occurring during the first (in plasma) and second (already directly in deposited films) stages of clustering. The proximity of the values of the Debye screening radius ($l_D = 175 \mp 30$ Å) and the maximum length of tunneling in solids (100−120 Å) to the cluster sizes, as well as the variety of structure and properties of the samples, make $La_{0.7}Sr_{0.3}MnO_{3-x}$ films studied in the paper attractive for a broader study of dimensional effects. The results of studies of a large number of samples with different structures and properties deposited simultaneously in a single technological process along a particle flux are useful for diagnosing low-temperature plasma and determining film parameters that are difficult or impossible to obtain using traditional methods. This was facilitated by the very logic of this study: any possible scenarios of plasma clustering and the formation of a cluster structure of films are immediately compared with the experiment.

Funding

This study was funded by the budget of Donetsk Institute for Physics and Engineering.

Conflict of interest

The authors declare that they have no conflict of interest.

References

[1] P.V. Kashtanov, B.M. Smirnov, R. Khippler. UFN **177**, *5*, 473 (2007). (in Russian).
[2] M. Panjan, A. Anders. J. Appl. Phys. **121**, *6*, 063302 (2017).
[3] V.E. Fortov, A.G. Khrapak, S.A. Khrapak, V.I. Molotkov, O.F. Petrov. UFN **174**, *5*, 495 (2004). (in Russian).
[4] W.D. Suranga Ruhunusiri, J. Goree. Physics of Plasmas **21**, *5*, 053702 (2014).
[5] B.B. Kadomtsev. Kollektivnye yavleniya v plazme. (Nauka, M. (1988). p. 303. (in Russian).
[6] V.D. Okunev, Z.A. Samoylenko, Yu.M. Nikolaenko, T.A. Dyachenko, A.S. Korneevets, E.I. Pushenko. Pis'ma v ZhTF **46**, *1*, 47 (2020). (in Russian).
[7] V.D. Okunev, Z.A. Samoylenko, H. Szymczak, T.A. Dyachenko, E.I. Pushenko. FTT **63**, *4*, 433 (2021). (in Russian).
[8] V.D. Okunev, Z.A. Samoilenko, H. Szymczak, R. Szymczak, V.V. Burkhovetski, S.J. Lewandowski. J. Appl. Phys. **113**, *16*, 164309 (2013).
[9] E.L. Nagaev. Phys. Rep. **346**, *6*, 387 (2001).
[10] L.P. Gor'kov and V.Z. Kresin. Phys. Rep. **400**, *3*, 149 (2004).
[11] A.L. Rakhmanov, K.I. Kugel, Y.M. Blanter, M.Y. Kagan. Phys. Rev. B **63**, *17*, 174424 (2001).
[12] V.D. Okunev, Z.A. Samoylenko, R. Szymczak, S.J. Lewandowski. ZhETF **128**, *1*, 150 (2005). (in Russian).
[13] V.D. Okunev, R. Szymczak, M. Baran, H. Szymczak, P. Gierłowski. Phys. Rev. B **74**, *1*, 014404 (2006).
[14] K.I. Kugel', A.L. Rakhmanov, A.O. Sboychakov, M.Yu. Kagan, I.V. Brodsky, A.V. Klaptsov. ZhETF **125**, *3*, 648 (2004). (in Russian).

[15] M.Yu. Kagan, K.I. Kugel, A.L. Rakhmanov, A.O. Sboychakov. Electronic Phase Separation in Magnetic and Superconducting Materials. Springer Series in Solid-State Sciences. **201**, (2024). 385 c.
[16] V.D. Okunev, Z.A. Samoylenko. Pis'ma v ZhETF **53**, *1*, 42 (1991). (in Russian).
[17] V.D. Okunev, Z.A. Samoylenko. Pis'ma v ZhTF **20**, *9*, 1 (1994). (in Russian).
[18] B.I. Shklovsky, A.L. Efros. Elektronnye svojstva legirovannykh poluprovodnikov. Nauka, M. (1979), p. 416. (in Russian).
[19] V.D. Okunev and H. Szymczak. J. Appl. Phys. **133**, *8*, 084301 (2023).
[20] V.D. Okunev, S.J. Lewandowski, T.A. Dyachenko, A. Abal'Oshev, P. Gierłowski, V.A. Isaev, FTT **53**, *1*, 15 (2011). (in Russian).
[21] V.D. Okunev, Z.A.Samoylenko, R. Szymczak, H. Szymczak, A. Szewczyk, A. Malinowski, J. Wieckowski, M. Wolny-Marszałek, M. Jezabek, I.A. Antoshina. ZhETF **153**, *6*, 945 (2018). (in Russian).
[22] V.D. Okunev, Z.A. Samoilenko, N.N. Pafomov, A.L. Plehov, R. Szymczak, H. Szymczak, S.J. Lewandowski. Phys. Lett. A. **373**, 8–9, 894 (2009).
[23] N. Mott, E. Davis. Eletronnye protsessy v nekristallicheskikh veshchestvakh, Mir, M. (1982). p. 663. (in Russian).
[24] E.L. Nagaev. UFN **166**, *8*, 833 (1996). (in Russian).
[25] David B. Wellbeloved, Peter M. Craven, John W. Waudby. Manganese and Manganese Alloys. Ullmann's Encyclopedia of Industrial Chemistry. **22**, 175 (2000).
[26] V.D. Okunev, Z.A. Samoylenko. FTT **33**, *10*, 2811 (1991). (in Russian).
[27] E.A. Neufeld, V.E. Arkhipov, N.A. Tumalevich, Ya.M. Mukovsky. Pis'ma v ZhTF **74**, 11–12, 630 (2001). (in Russian).
[28] E.L. Ivchenko. UFN **182**, *8*, 869 (2012). (in Russian).
[29] I.M. Lifshits. UFN **83**, *8*, 617 (1964). (in Russian).

Translated by A.Akhtyamov